Supporting Information

Synthesis of Tantalum Oxide Nanoparticles for Imaging Articular Cartilage Using X-Ray Computed Tomography: Visualization of Ex vivo / In vivo Murine Tibia and Ex vivo Human Index Finger Cartilage

Jonathan D. Freedman,[1,4] Hrvoje Lusic,[2] Brian D. Snyder,[4] Mark W. Grinstaff [1-3*]
Departments of [1]Pharmacology, [2]Chemistry and [3]Biomedical Engineering, Boston University, Boston, MA
[4]Center for Advanced Orthopaedic Studies, Beth Israel Deaconess Medical Center, Harvard Medical School, Boston, MA

Experimental Section

All chemicals and reagents were purchased from Sigma-Aldrich (St. Louis, MO) unless otherwise specified.

1. Synthesis of Nanoparticles (NPs) **1**, **2** & **3**.

The synthetic procedure was adapted from Hyeon[1] and Bonitatibus et al.[2] Briefly, Ta_2O_5 NP cores were formed with tantalum(V) ethoxide in n-propanol and deuterated water, using isobutryic acid to control size. The appropriate silane ligand was subsequently added, followed by refluxing of the reaction in n-propanol. Appropriate workup and purification yielded the desired NPs.

Silane ligand derivatives were purchased from Gelest, Inc. (Morrisville, PA).

- 2-(carbomethoxy)ethyl trimethoxysilane (Gelest Product #: SIC2072.0; CAS: 76301-00-3)
- (2-diethylphosphatoethyl)triethoxysilane (Gelest Product #: SID3412.0; CAS: 757-44-8)
- (3-triethoxysilylpropyl)-*t*-butyl carbamate (Gelest Product #: SIT8186.5; CAS: 137376-38-4)

The NPs were purified by dialysis (3,500 MWCO, Snakeskin®, Thermo Sci., Billerica, MA) over 72 h, and by filtration through 0.22 μm PES membrane (Corning Inc, Corning, NY).

Ethyl phosphonate tantalum oxide NPs (1). The NPs were synthesized according to the literature procedure.[3] ^{1}H NMR (400 MHz, D_2O): δ =0.69 (br s, 2 H), 1.19 (br s, 3 H), 1.72 (br s, 2 H), 4.00 (br s, 2 H). ^{31}P NMR (162 MHz, D_2O): δ = 36.3 (br s). FTIR (cm^{-1}): 1444 (weak), 1412 (weak), 1273 (weak), 1215 (strong), 1165 (medium), 1094 (weak), 1020 (very strong), 938 (very strong), 777 (strong). ICP-AES: Ta/Si (wt/wt) 2.08 ± 0.02.

(*n*-Propylamine HCl salt) tantalum oxide NPs (2). Isobutyric acid (0.44 mL) and D_2O (0.5 mL) were added to an *n*-propanol (34 mL) solution. Tantalum(V) ethoxide (1.87 g, 1.19 mL) was added dropwise at a rate of 0.2 mL/min, and the solution was left to stir for 16 h at rt, under N_2 atmosphere. The solution was then diluted by addition of *n*-propanol (20 mL), followed by addition of *tert*-butyl 3-(triethoxysilyl)propylcarbamate (5 g) in *n*-

propanol (15 mL) at a rate of 1 mL/min. The reaction was subsequently refluxed for 2 h, and then cooled to rt. Next, NH_4OH (0.1 M, 250 μL) was added to the solution, and the reaction was stirred for 16 h at rt. Subsequently, H_2O (40 mL), and aq. HCl (1.2 M, 10 mL) were added to the flask dropwise over 20 min. The reaction was then allowed to proceed at 50 °C for 48 h. The reaction was cooled to rt, and filtered through a 0.22 μm membrane, and the volatiles were evaporated. The residue was redissolved in MeOH (50 mL), and cooled to 0 °C. A solution of 2 N HCl (50 mL) was added to the flask and the reaction was stirred at rt for 48 h. The solution was neutralized to pH 7 by addition of Na_2CO_3, filtered through a 0.22 μm membrane, and then transferred into dialysis tubing (MWCO 3.5 kDa). The product was dialyzed over 72 h, with frequent water changes. Removal of volatiles by lyophilization afforded **2** as white powder. ^{1}H NMR (400 MHz, D_2O): δ =0.53 (br s, 2 H), 1.64 (br s, 2 H), 2.89 (br s, 2 H). ^{13}C NMR (100 Hz, D_2O): δ = 9.7, 21.0, 41.7. FTIR (cm^{-1}): 3320 (weak), 2919 (very strong), 1611 (medium), 1502 (medium), 1210 (weak), 1044 (weak), 922 (strong), 802 (weak). ICP-AES: Ta/Si (wt/wt) 4.96 ± 0.06.

Sodium propanoate tantalum oxide NPs (3). Isobutyric acid (0.44 mL) and D_2O (0.5 mL) were added to an *n*-propanol (34 mL) solution. Tantalum(V) ethoxide (1.87 g, 1.19 mL) was added dropwise at a rate of 0.2 mL/min, and the solution was left to stir for 16 h at rt, under N_2 atmosphere. The solution was diluted by addition of *n*-propanol (20 mL), followed by addition of methyl 3-(triethoxysilyl)propanoate (5 g) in *n*-propanol (15 mL) at a rate of 1 mL/min. The reaction was subsequently refluxed for 2 h, and then cooled to rt. Next, NH_4OH (0.1 M, 250 μL) was added to the solution, and the reaction was stirred for 16 h at rt. Subsequently, H_2O (40 mL), and aq. HCl (1.2 M, 10 mL) were added to the flask dropwise over 20 min. The reaction was then allowed to proceed at 50 °C for 48 h. The reaction was cooled to rt, and filtered through a 0.22 μm membrane, and the volatiles were evaporated. The residue was redissolved in MeOH (50 mL), and cooled to 0 °C. DI water (50 mL) was added the flask, and the pH was adjusted to pH 10, by addition of Na_2CO_3 and the reaction was stirred at 40 °C for 48 h. The solution was neutralized to pH 7 by addition of 1 N HCl, filtered through a 0.22 μm membrane, and then transferred into dialysis tubing (MWCO 3.5 kDa). The product was dialyzed over 72 h, with frequent water changes. Removal of volatiles by lyophilization afforded **3** as white powder. ^{1}H NMR (400 MHz, D_2O): δ =0.59 (br s, 2 H), 2.00 (br s, 2 H). ^{13}C NMR (100 Hz, D_2O): δ = 9.2, 30.6, 185.8. FTIR (cm^{-1}): 3265 (weak), 2927 (weak), 1656 (weak), 1562 (strong), 1410 (strong), 1304 (weak), 1187 (weak), 1033 (medium), 912 (very strong). ICP-AES: Ta/Si (wt/wt) 2.64 ± 0.05.

2. Dynamic Light Scattering (DLS) Size Characterization

The hydrodynamic size of the nanoparticles was measured by dynamic light scattering (DLS) at 25 °C using the Brookhaven Instruments 90 Plus Particle Sizer (Brookhaven Instruments, Holtsville, NY). Samples were prepared in Orion pH Buffer Solutions (Thermo Sci., Billerica, MA). Hydrodynamic size was based on 5 measurement Z-average/-effective of intensity-based distribution.

3. Zeta Potential Characterization

The zeta potential of the nanoparticles was measured using the Brookhaven Instruments ZetaPALS Zeta Potential Analyzer (Brookhaven Instruments, Holtsville, NY). The same samples used for DLS size characterization were used to determine zeta potential. Each sample was subjected to 5 runs each consisting of 20 cycles with auto correction for voltage.

4. Scanning Electron Microscopy (SEM) & Transmission Electron Microscopy (TEM)

Samples for SEM were prepared by allowing a 10 μL droplet of 1 mg/mL nanoparticle solution to dry on a silica wafer connected to an aluminum sample stub. Samples were imaged on a Zeiss SUPRA 40VP (Carl Zeiss Microscopy LLC, Oberkochen, Germany) field emission scanning electron microscope using an accelerating voltage of 2 kV. Particle size was analyzed using Image J (NIH, Bethesda, MD), where all particles in a representative image were sized to characterize the effective feret's diameter of the particles.

Samples for TEM were prepared on 20 nm thick low-stress SiN_x membranes (50x50 μm square) supported on a silicon chip. NPs were deposited by allowing a 10 mL droplet of 1 mg/mL nanoparticle solution to dry to on the windows. Samples were imaged using a transmission electron microscope (JEOL 2010F) at 200 kV. Micrographs were recorded with a Gatan Model794 Multi Scan Camera with 2x2 binning at 150kx magnification.

We thank the Center for Nanoscale Systems at Harvard University for imaging support.

5. Fourier Transform Infrared Spectroscopy (FTIR) Measurements

FTIR spectra were obtained on dried Ta_2O_5 NPs samples, using Thermo-Nicolet Nexus 670 FTIR E.S.P. instrument, equipped with Miracle ZnSe ATR prism (Thermo Sci., Billerica, MA).

6. Inductively Coupled Plasma – Atomic Emission Spectroscopy (ICP-AES) Measurements

The ICP-AES were obtained on Ultima C by HORIBA Jobin-Yvon, equipped with a monochromator. Reference standards were made from mono-elemental standards, at a range of concentrations (from 0.5 to 75 ppm) in order to define a calibration curves for both Si and Ta. NP samples were digested in 2% nitric acid. Emissions at the following wavelengths: 226.230, 263.558, 268.511 and 279.770 nm were measured for Ta. Emissions at 221.667, 251.611 and 252.851 nm were measured for Si. Measurements at the different wavelengths were usually consistent within ~1%.

7. Dissection of Mouse Tibia

Healthy BALB/c mice were dissected under an operating microscope. The knee was disarticulated and all soft tissue, except for cartilage, removed. The intact bone and cartilage were stored frozen in 400 mOsm saline with antibiotics (Anti-Anti, Life

Technologies, Bedford, MA) and protease inhibitors (EDTA & Bezamidine HCl, Sigma, St. Louis, MO) before use.

8. Nanoparticle Solutions for Cartilage Immersion

NPs (40 mg) were added to deionized water (1 mL). Solutions were adjusted to pH 7.4 with 4.0 M sodium hydroxide and to 380-420 mOsm with sodium chloride.

9. Murine Tibia μCT Imaging

Imaging of murine tibia was performed on a μCT (μCT 40, Scanco AG) at 6 μm resolution. The mouse tibias were randomly assigned to be immersed in NP **1**, **2** or **3**. For contrast agent diffusion-in, tibias were scanned at baseline and then immersed in 500 μL of NP solutions (40 mg NP/mL. pH 7.4, 380-420 mOsm) and rescanned at 6, 12, 24 and 48 hours.

10. Human Finger μCT Imaging

The metacarpal phalangeal joint of a human index finger was dissected and the surrounding soft tissue removed leaving cartilage and bone. The defect was photographed with an iPhone 5 (Apple, Cupertino, CA) and contrast imaging performed on a μCT (μCT 40, Scanco AG) at 36 μm^3 resolution.

11. Image Processing of Murine and Human μCT Images

DICOM images were imported into Analyze 11 (BIR, Mayo Clinic, MN) for post-processing. Quantitative measurements were made with the following procedure: Images were registered to their corresponding baseline scan. The baseline scan was used to create an object map of the bone in the Volume Edit tool. This bone object map was locked and used with the corresponding 48 hour scan to create object maps of the medial and lateral tibial plateaus. The resulting object map could then be used for all time points. The Region of Interest tool was used to sample each image.

12. Diffusion-in & out Kinetics Data Processing

Diffusion-in curves were fit using MATLAB 2011b (Mathworks, Natick, MA) using the curve-fit tool (cftool) toolbox. Data was fit linearly except for diffusion-in kinetics of NP **2**, which was fit to the function $f(t)=A(1-e^{-t/\tau})$.

13. Cell Maintance of NIH3T3 Murine Fibroblast Cells for Toxicity Stuides

NIH3T3 murine fibroblast cells were maintained in Dulbecco's Modified Eagle Media supplemented with 10% bovine calf serum and 1% penicillin/streptomycin. Cells were maintained in a humidified atmosphere at 37 °C and 5% CO_2. Subconfluent cells were harvested and seeded on 96 well plates at 20,000 cells/well for use in *in vitro* cytotoxicity

studies.

14. *In vitro* cytotoxicity study

NIH3T3 fibroblasts were allowed a 4 hour exposure to concentrations of 40, 20, and 10 mg of NP/mL & 160 mg I/mL and 80 mg I/mL of ioxaglate (Hexabrix 320, Mallinckrodt Inc, St. Louis, MO) in phosphate free DMEM (Catalog #: 11971-025, Life Technologies, Carlsbad, CA) and then replaced with the maintenance formulation media for 18 hours. Cells were maintained in a humidified atmosphere at 37 °C and 5% CO_2. After exposure, cell viability was tested using a colorimetric MTS [3-(4,5-dimethylthiazol-2-yl)-5-(3-carboxymethoxyphenyl)-2-(4-sulfophenyl)-2*H*-tetrazolium] cell proliferation assay (Sigma, St. Louis, MO) and absorbance read at 490 nm on a Beckman-Coulter AD 340 Plate Reader (Brea, CA). Cell viability in each well was calculated as the percentage of the positive control absorbance.

15. Histology

Histology was performed by the Beth Israel Deaconess Medical Center Histology Core. Standard protocols were used for fixing, sectioning, and staining the tissue samples. Murine samples were stained with Hematoxylin and Eosin (H&E), Masson's Trichrome Stain (MTS) and Safranin-O with fast green (Saf-O). Images were taken with an iPhone 5 (Apple, Cupertino, CA) through a 10x microscope objective.

16. *In vivo* Imaging

All procedures were approved by the institutional animal care and use committee at Beth Israel Deaconess Medical Center. The male Wistar rat (Charles River Laboratories, Wilmington, MA) was anesthetized by isoflurane. The rat received isoflurane for the entire duration of the experiment. 100 μL of NP **2** (40 mg NP/mL) was administered to the right knee joint through the suprapatellar recess in aseptic conditions. A contrast enhanced scan was obtained by using a peripheral quantitative CT scanner (XCT Research SA+; Stratec Medizintechnik, Pforzheim, Germany). Sections were acquired at 100 μm^2 in-plane resolution, 50 kVp tube voltage, and 300 μA current and imported into Analyze for analysis. The rat was euthanized and both legs excised and scanned *ex vivo* on a μCT (μCT 40, Scanco AG) at 36 μm^3 resolution and imported into Analyze for analysis.

Supplementary Results and Discussion

I. Contrast Agent Mechanism

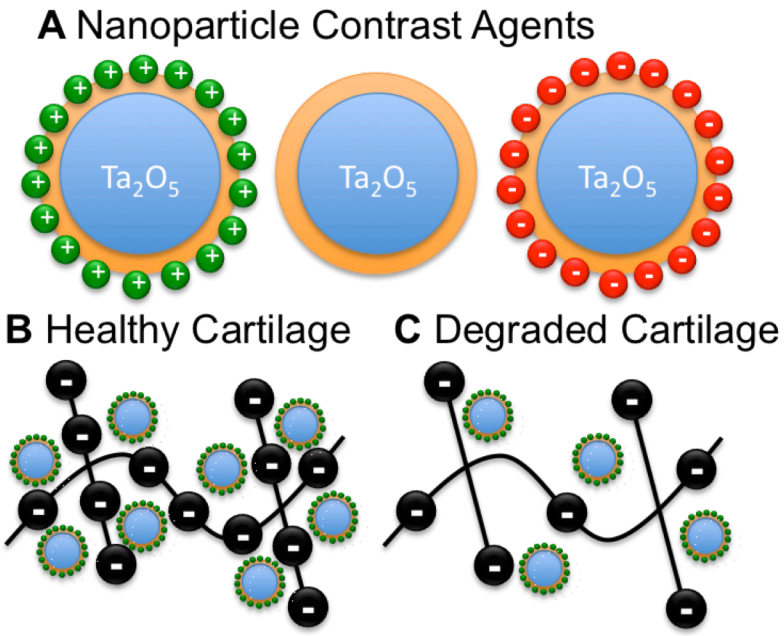

Figure S1. (A) General structure of proposed nanoparticles (NPs) with tantalum oxide core (blue), silane ligands (orange) and charged groups (green/red). (**B&C**) Cationic NPs are attracted to the negatively charged glycosaminoglycans (GAG; black) in cartilage. High levels of GAG in healthy tissue (**B**) will attract more positive contrast than low levels of GAG in degraded tissue (**C**).

II. NMR Characterization of NPs **1**, **2** & **3**.

The NMR analysis of the NPs showed existence of a uniform species for the phosphonate NPs. The ^{1}H NMR peaks, as previously reported[1-4] by others for these types of materials, appear to be broadened. Likewise, ^{31}P NMR (for the phosphonate nanoparticle), and ^{13}C NMR exhibited expected resonances, albeit also giving broadened peaks. The obtained NMR-shift values roughly correspond to the shifts expected for the non-conjugated silane structures.

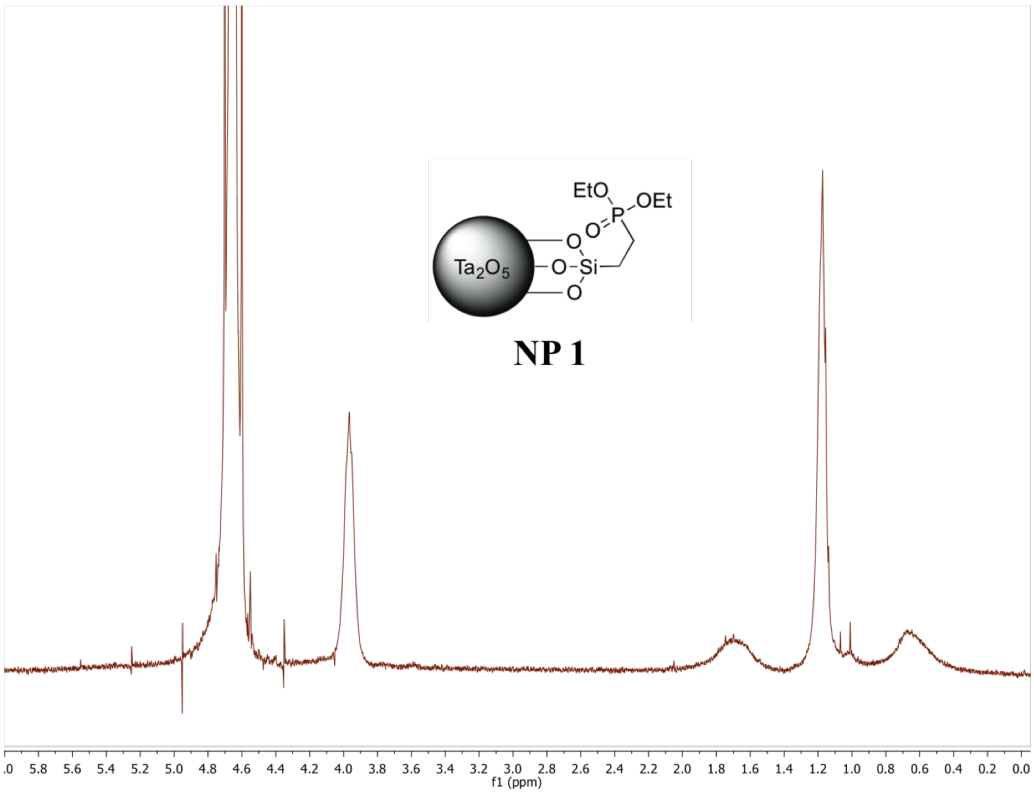

Figure S2. ^{1}H NMR spectrum of NP **1**.

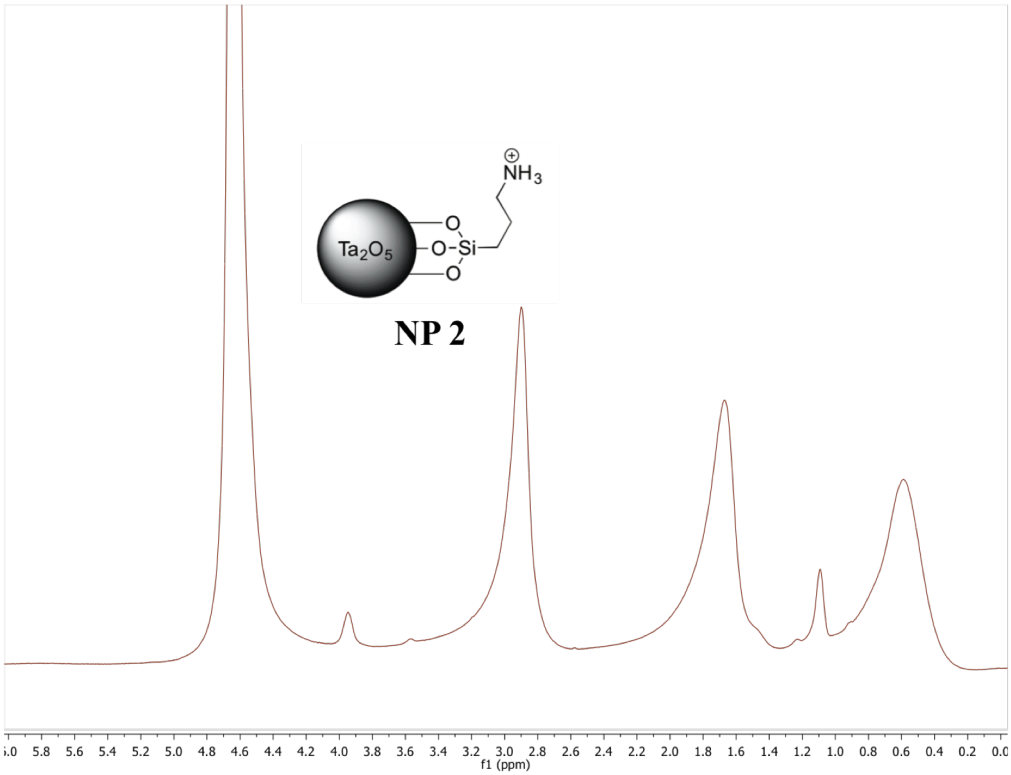

Figure S3. ^{1}H NMR spectrum of NP **2**.

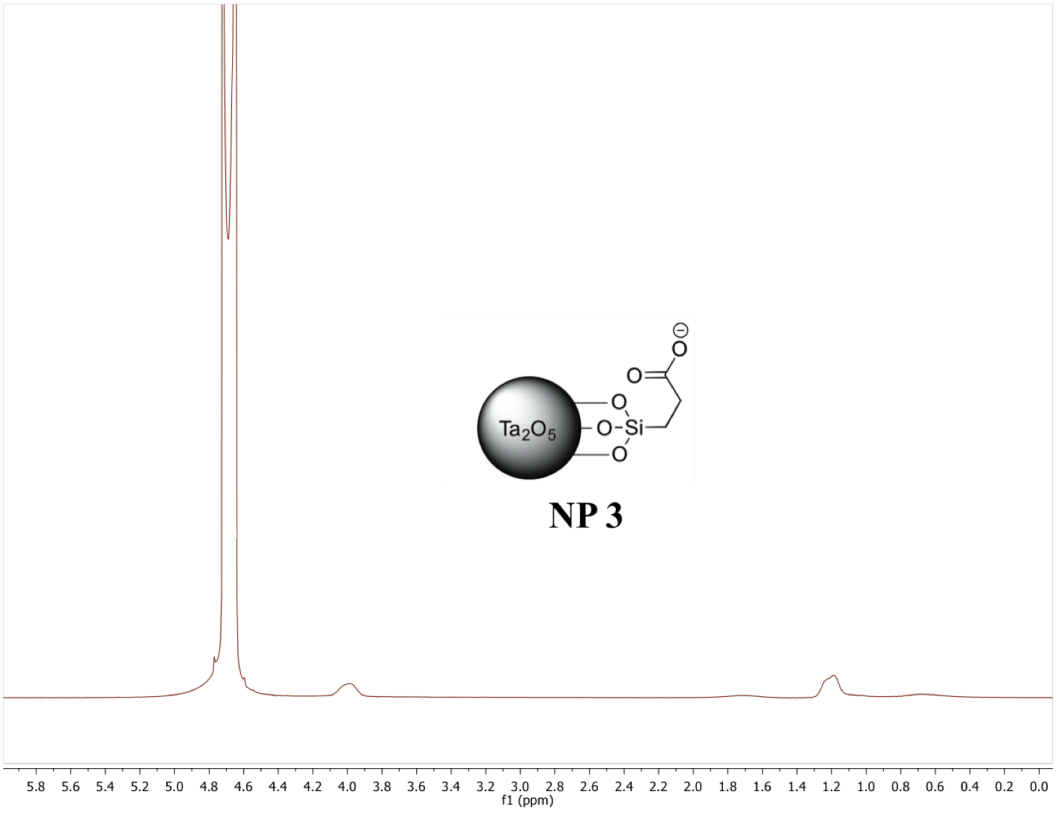

Figure S4. ^{1}H NMR spectrum of NP **3**.

III. FTIR Characterization of NPs **1**, **2** & **3**.

The FTIR spectrum of the NP **3** showed strong absorbance peaks at 1560 cm^{-1} and 1410 cm^{-1}, respectively corresponding to the asymmetric (1650-1550 cm^{-1}) and symmetric (1500-1400 cm^{-1}) C=O stretches characteristic of carboxylate ions. The FTIR spectrum of NP **2** exhibited a very strong absorption band at 2919 cm^{-1} and a couple of medium-absorption bands at 1611 and 1502 cm^{-1}, respectively corresponding to the N-H stretch (3150-3000 cm^{-1}) and N-H bend (1600-1500 cm^{-1}) regions characteristic of the primary ammonium ions.

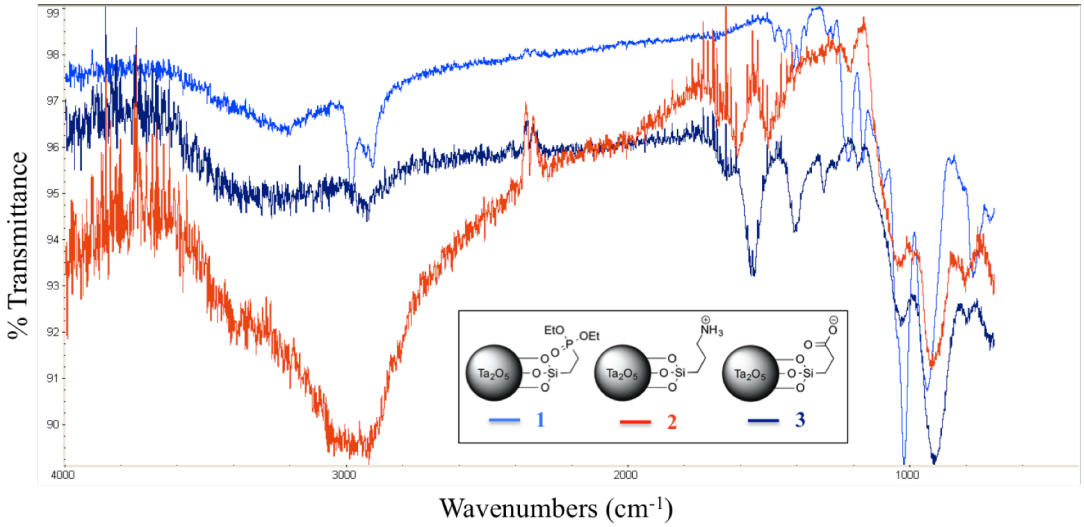

Figure S5. FTIR spectra of the Ta_2O_5 nanoparticles. (Light blue = NP **1**, Red = NP **2**, Dark blue = NP **3**.)

IV. ICP-AES Characterization of NPs **1**, **2** & **3**.

The ICP-AES analysis showed that the Ta/Si (wt/wt) ratio in NP **1** was similar to the previously reported values; i.e. ~2.07. The ratio of Ta/Si was found to be slightly higher in NP **3**; i.e. ~2.64, but within range of that observed for NP **1**. However, the ratio of Ta/Si in NP **3** was significantly higher; i.e. ~4.96, meaning that the degree of silane coating is roughly half of that observed for NPs **1** and **3**. This result could be due to the rather harsh conditions required for the removal of the Boc-protecting group on the amine functionality, resulting in less Si on the surface.

V. DLS Size and Zeta Potential Characterization of NPs **1**, **2** & **3**.

Zeta potential measurements on the NPs afforded values that were in line with our expectations. At physiological pH 7.4 the zeta potential values of the NPs significantly differ (Table S1) based on the chemical composition of the coating. NP **2** exhibits a positive zeta potential, while NP **3** exhibits a much more negative zeta potential than NP **1**. We presume that the "neutral" NP **1** exhibits a slight intrinsic negative zeta potential due to the presence of the oxide groups on the particle surface (Table S1).

Table S1. Summary of DLS sizing and zeta potential values in different conditions.

		NP **1**	NP **2**	NP **3**
PBS 1x, SDS 0.1% (~290 mOsm), pH 7.4	Size (nm)	6.50	3.30	4.96
	Zeta (mV)	-1.14	7.58	-19.07

VI. Electron Microscopy (EM)

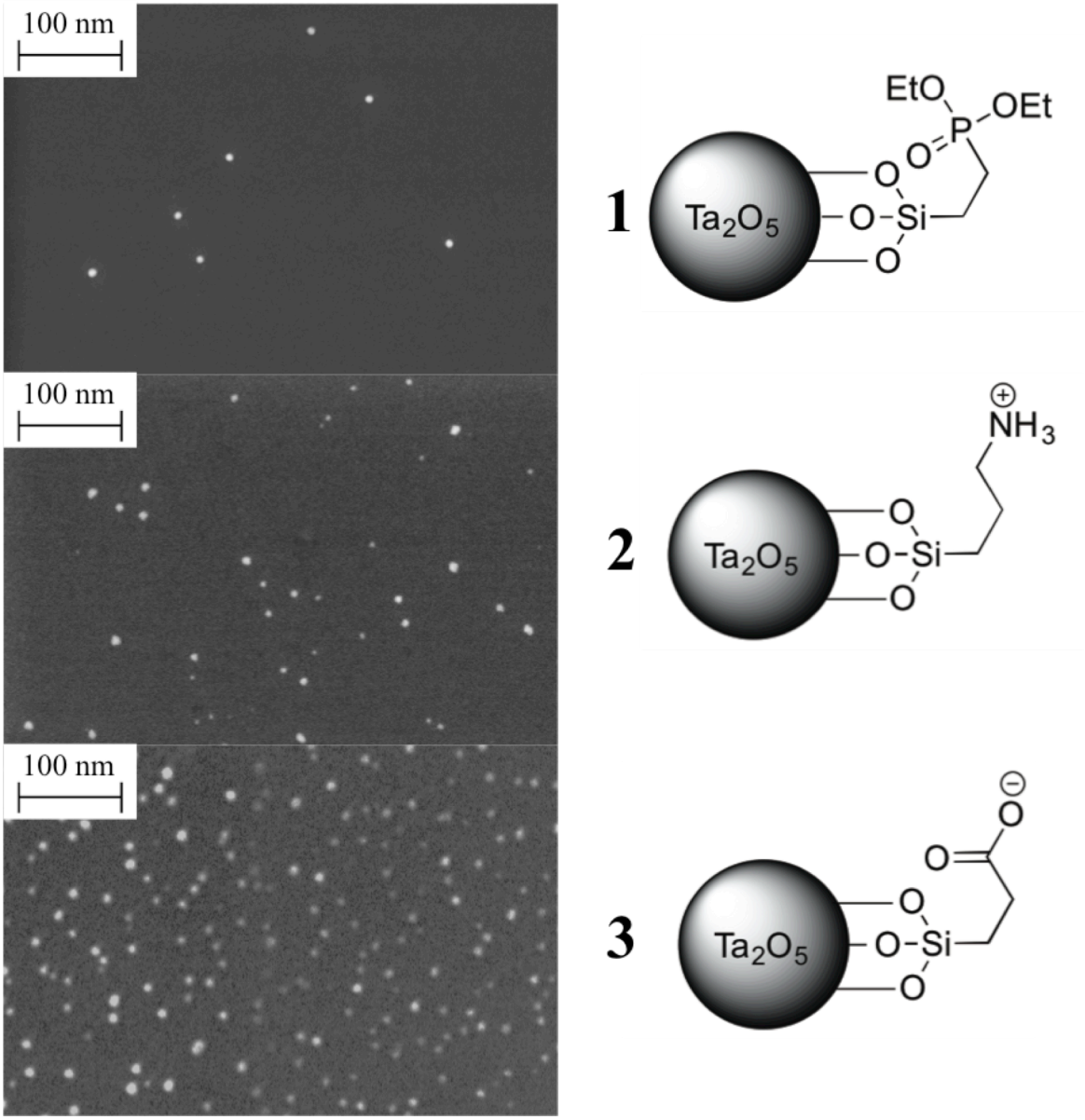

Figure S6a. Scanning EM images of Ta_2O_5 NPs with three different silane ligands. D±S.D.: NP **1** = 7.3±2.9, NP **2** = 6.0±4.4, NP **3** = 9.6±3.3.

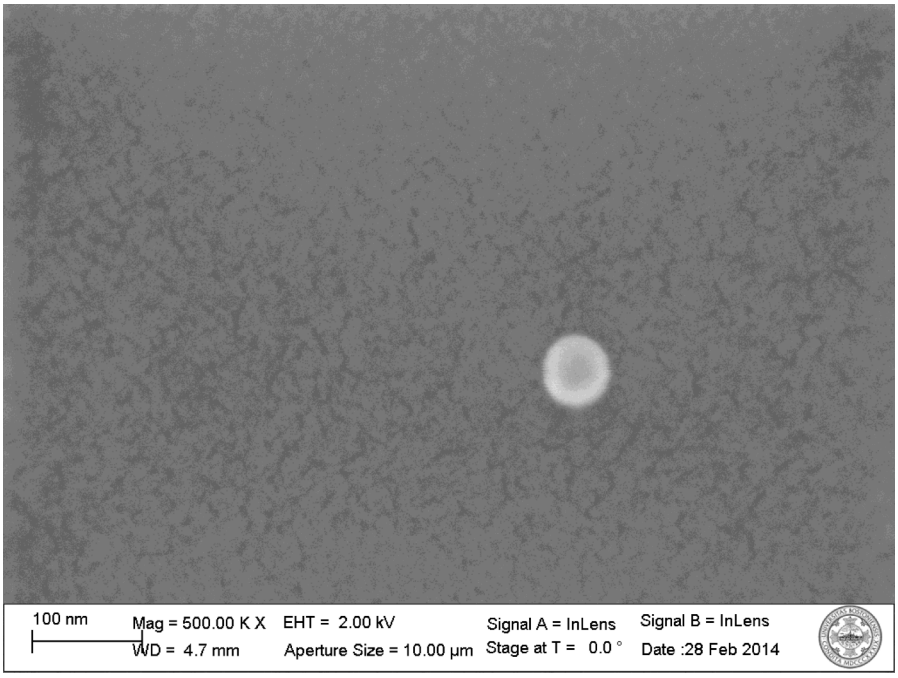

Figure S6b. High Resolution scanning EM image of an Au/Pd sputter coated NP core. The sputter coating greatly increases the observed size.

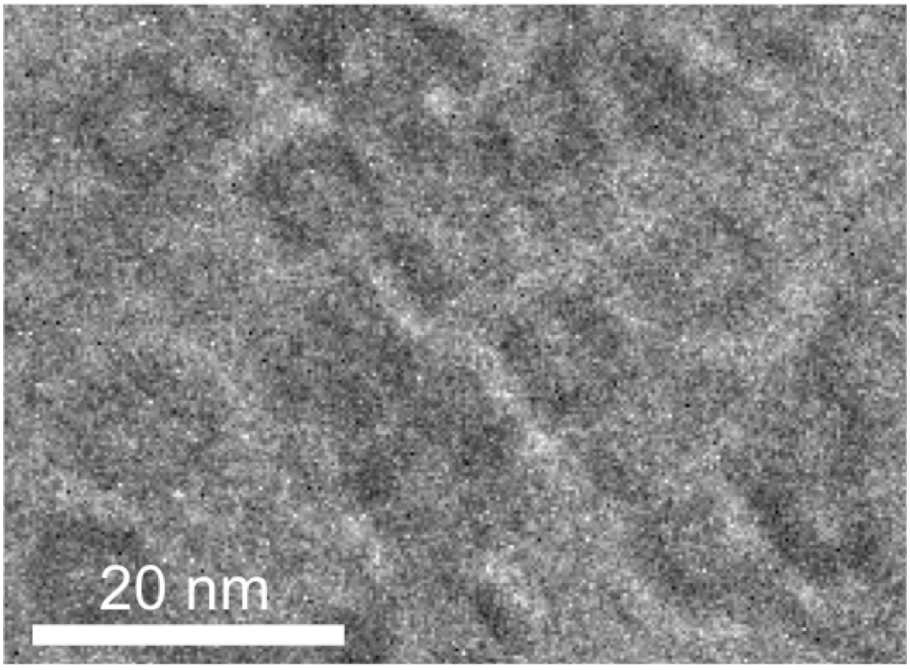

Figure S6c. Transmission EM image depicting the NP cores.

VII. *In vitro* phantom studies of NP attenuation

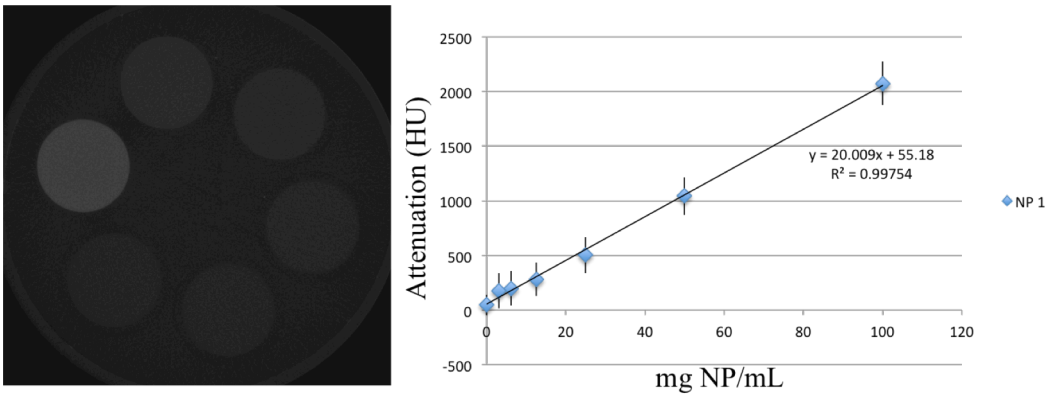

Figure S7. *In vitro* phantom studies of aqueous solutions of the synthesized nanoparticles were performed. CT reconstruction images visually show an increasing brightness with increasing NP concentration (**Left**). The quantitative X-ray attenuation properties of the Ta_2O_5 NPs (**Right**); n=3 mean±standard deviation.

VIII. Diffusion kinetics of NPs **1, 2 & 3** in and out of murine tibia cartilage.

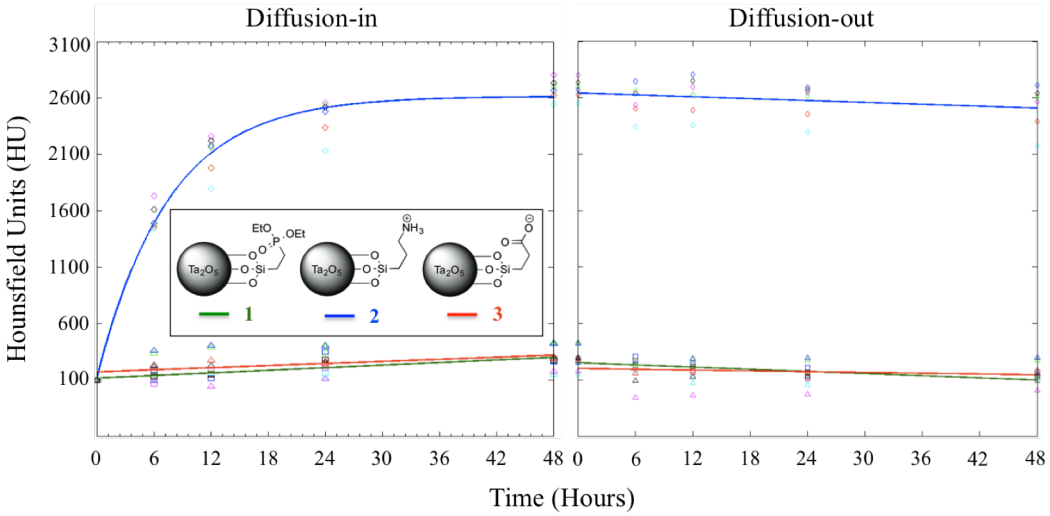

Figure S8. Diffusion-in and diffusion-out kinetics of NP contrast agents. The NPs were allowed to incubate in 40 mg NP/mL for 48 hours and then incubate in saline for 48 hours. NP **2** (blue line) produces greater attenuation than NPs **1** (green line) or NP **3** (red line) after 48 hours. The strong Coulombic interactions between positively charged NP **2** and the negatively charged GAG chains result in a significantly higher uptake into the cartilage tissue. In fact, the interactions are so strong that NP **2** remains embedded in the cartilage tissue for at least 48 h after incubation in a saline washout.

IX. Murine Histology

Our target of interest is articular (hyaline) cartilage. This tissue is composed of water (68-85% by wt), collagen (10-20% by wt), glycosaminoglycans (5-10% by wt) and is sparsely cellular. This can be seen in a high resolution (40x objective) Safranin-O/Fast Green stained histology section of murine tibial cartilage (Figure S9b). In this image, the glycosaminoglycan content is stained pink, the cells purple and the bone green. The cells display a sparse punctate pattern in the cartilage matrix. When in immersed in NP **2**, contrast appears throughout the tissue, similarly to the pinkly stained glycosaminoglycan content in the histology image which is distributed throughout the matrix as well as surrounding the cells. Since Safranin-O is a cationic dye, it is representative of the potential distribution of NP **2**.

The nanoparticles functionalized with primary amines (NP **2**) were injected intra-articularly directly into the knee of a live Wistar rat. The rat underwent *in vivo* imaging and recovered from anesthesia without distress or adverse events. No synovitis was observed during or after the intra-articular injection. The rat was subsequently euthanized, the limb imaged *ex vivo,* and the tissue prepared for histology. To assess the presence of synovial membrane cell hyperplasia, vascular dilatation, or inflammatory cell infiltrate, H&E stained histological sections, were obtained. The results were comparable to non-treated, healthy control samples using an established semi-quantitative grading scale to evaluate the cartilage tissue samples for structural changes to the articular cartilage (surface irregularities, pannus formation and/or clefting) and chondrocytes (hypercellularity, cloning, empty lacunae) as well as to the synovial tissue. A histology image of the injected joint can be seen in Figure S9c.

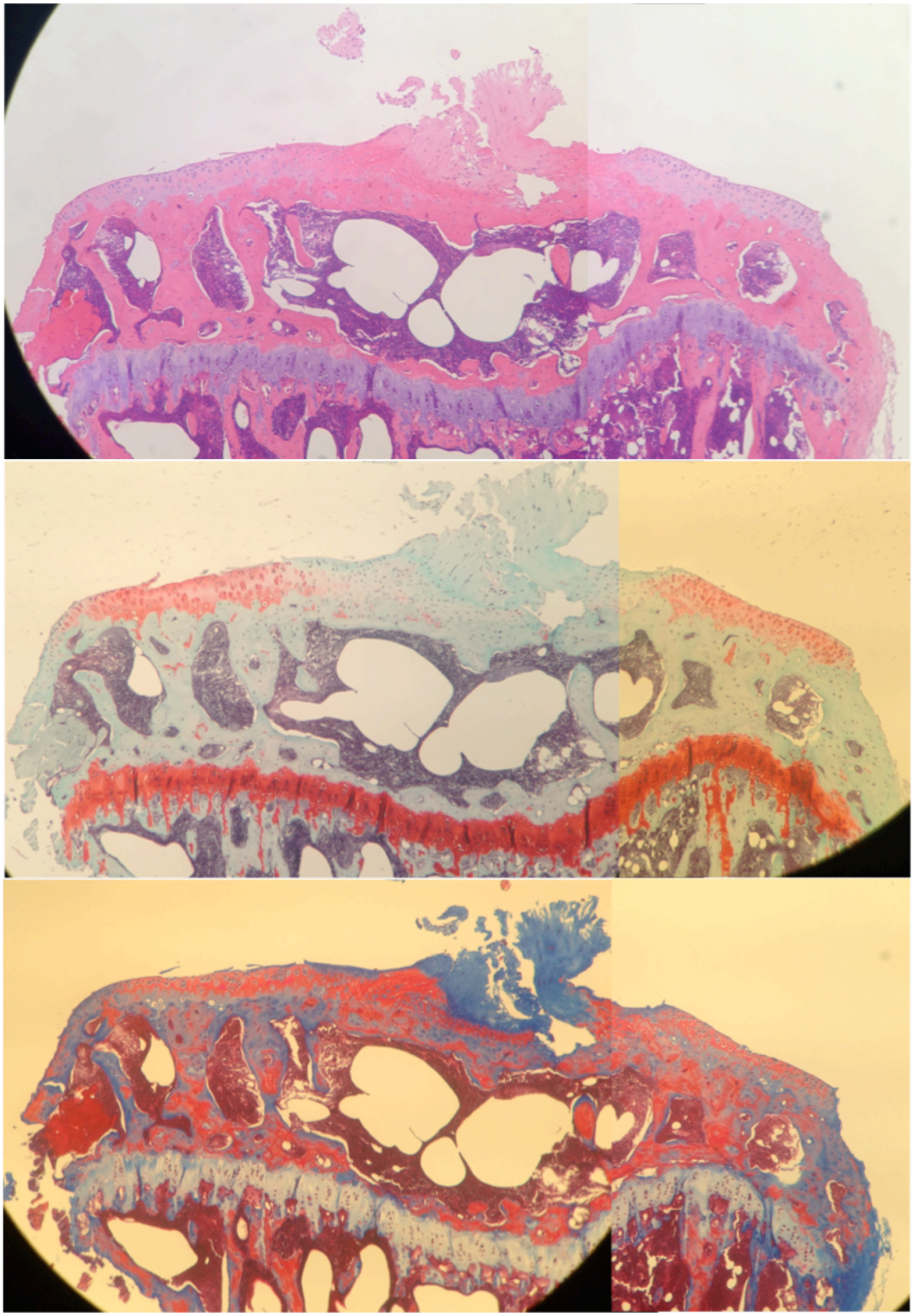

Figure S9a. H&E (Top), Saf-O (Middle), and MTS (Bottom) histology slides of mouse tibia in the coronal view. Saf-O shows pink staining of glycosaminoglycans in cartilage.

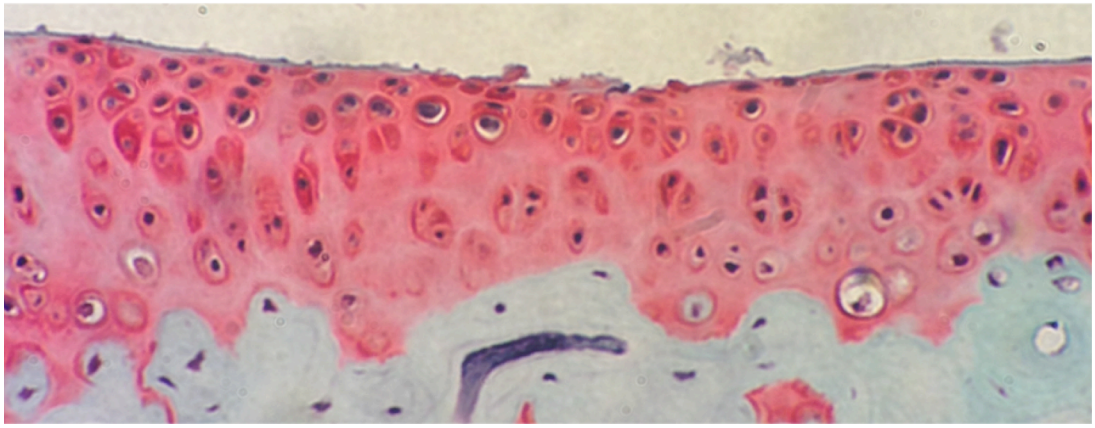

Figure S9b. High Resolution (40x objective) of Safranin-O stained murine tibial cartilage. This stains cells purple, bone green and glycosaminoglycans pink.

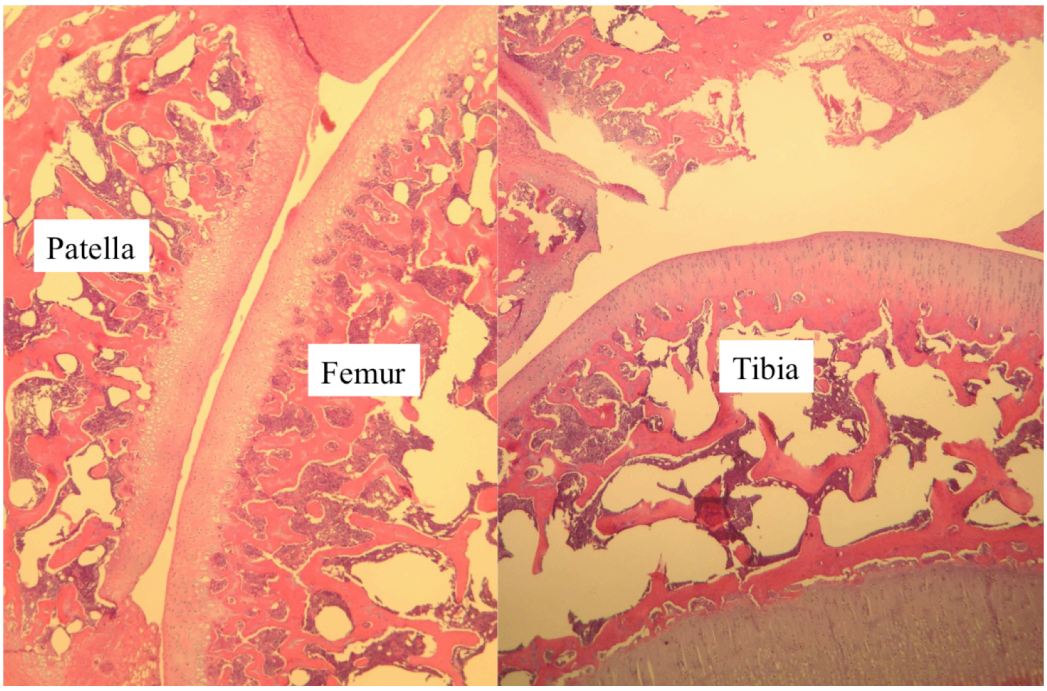

Figure S9c. H&E stained histology section of the rat knee joint after injection with NP **2**. The cartilage appeared normal with no signs of inflammation or synovitis.

X. Gross photography of the distal metacarpal phalangeal (MCP) joint

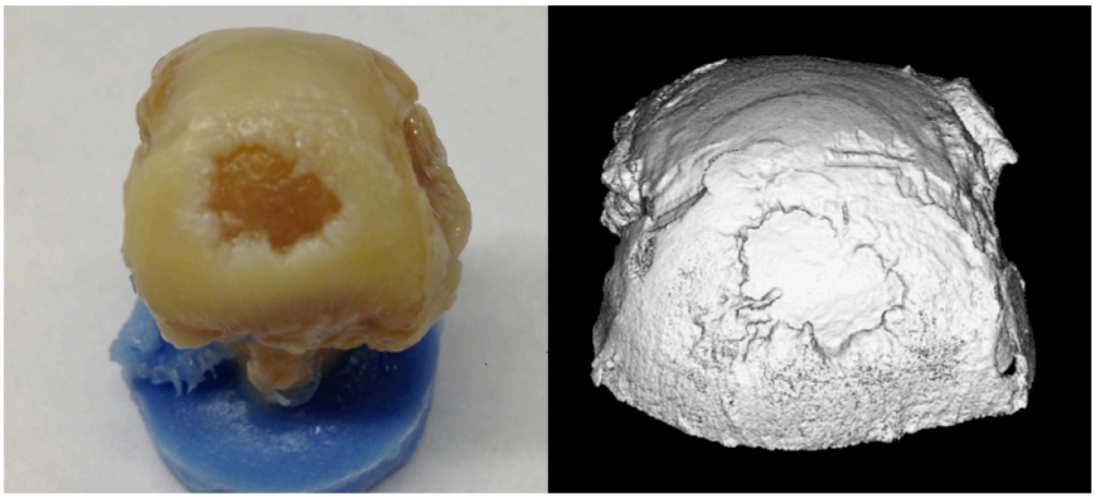

Figure S10. Gross inspection (Left) of the distal MCP joint. A large defect with exposed bone and irregular cartilage edges is observed. The defect can be visualized by contrast enhanced CT after 24 hours of immersion in NP **2** (Right).

XI. Cytotoxicity of NPs **1**, **2** & **3** against 3T3 fibroblasts.

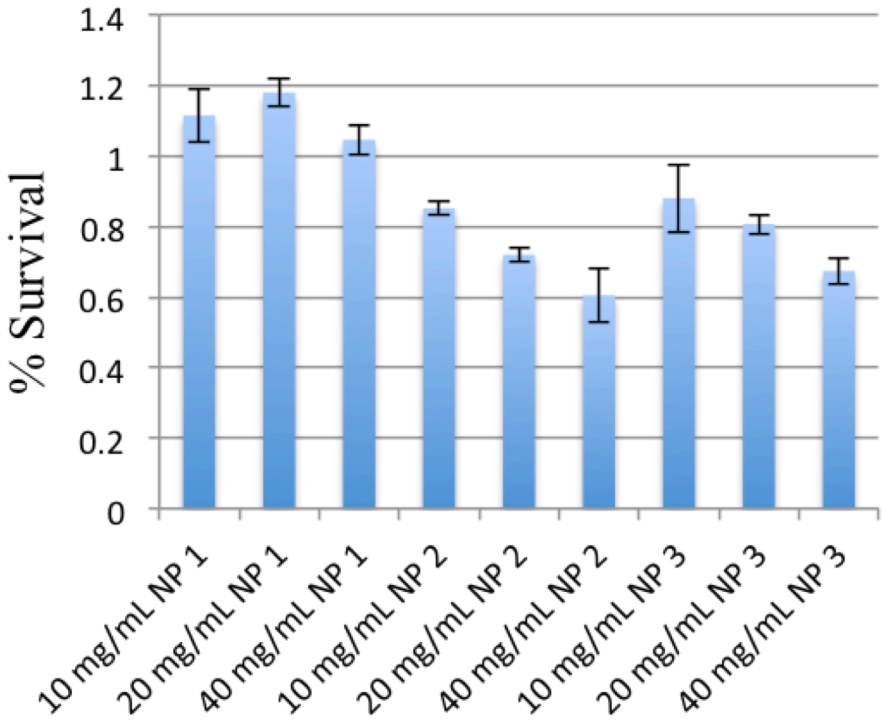

Figure S11. Cytotoxicity of a 4 hour exposure of NPs **1**, **2** & **3** against 3T3 Fibroblast cells by MTS assay; n = 3. Mean±standard deviation.

Evaluation of toxicity of the three types of NPs by MTS assay in 3T3 Fibroblast cells in a four hour exposure in phosphate free media. NP **1** did not exhibit any appreciable toxicity, as has already been demonstrated previously iv in rats[1-4]. However, we observed an almost equivalent level of toxicity for both NP **2** & **3**. This toxicity is most probably due to the tendency of charged NPs to interact with proteins and other biological structures. The result also suggests that further optimizations of the NP coating composition and adjustment of the coating charge are necessary before such imaging agents can be used *in vivo*. Nevertheless, the higher affinity of NP **2** for the cartilage tissue can be exploited so that lower concentrations of imaging agent may be used in a study, thus lowering the potential toxic side-effects.

XII. Cytotoxicity of Ioxaglate (Hexabrix)

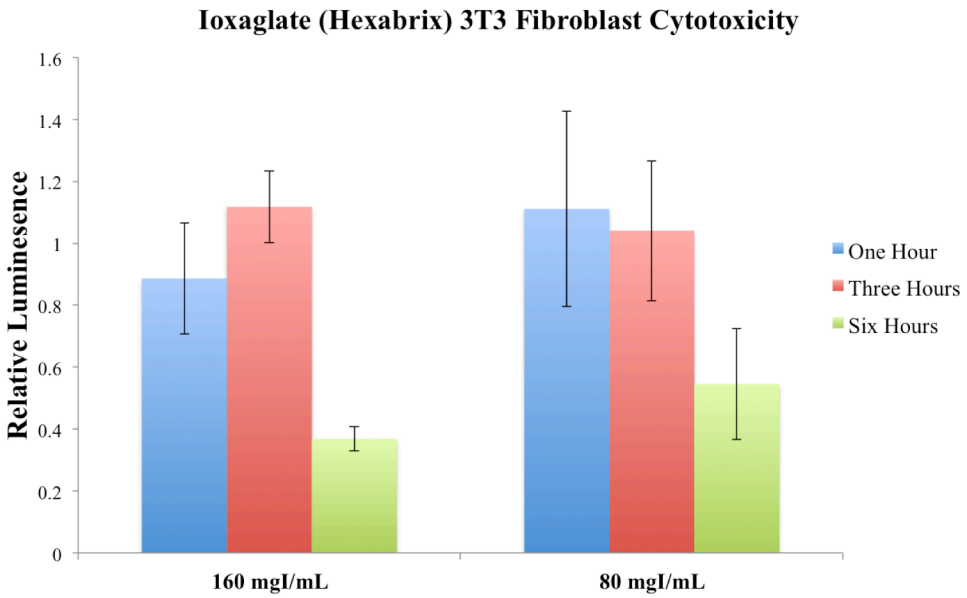

Figure S12. Cytotoxicity of ioxaglate (Hexabrix) against 3T3 fibroblasts after 1, 3 and 6 hour exposures; n = 3. Mean±standard deviation.

XIII. Optimization of charge density and biocompatibility.

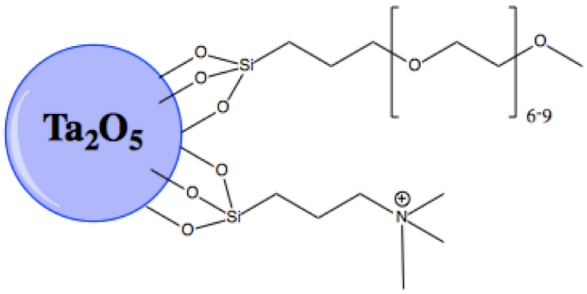

Figure S13a. The quaternary ammonium ion was chosen to ensure a fixed positive charge and a (short) pegylated ligand was chosen to improve biocompatibility. The NP was synthesized using a similar protocol to NP **1**.

The optimized NP (~8nm in size; Zeta potential in deionized water = 13.22±2.44. Zeta potential in PBS 0.8±3.8) showed the same affinity for cartilage and displayed no cytotoxicity over 24 hours to 3T3 fibroblasts.

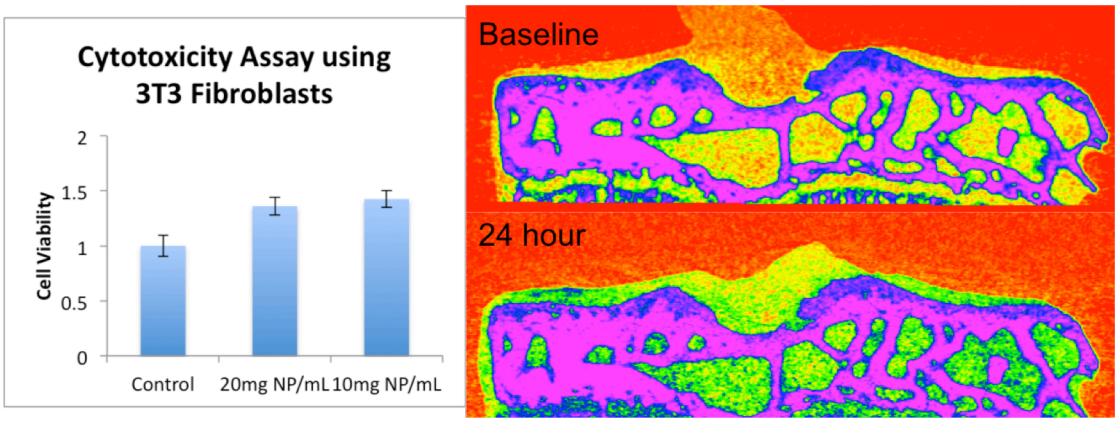

Figure S13b. Left: 24-hour exposure of 50:50 (PEG:ammonium) functionalized nanoparticles displayed no cytotoxicity to 3T3 fibroblasts. Right: CT coronal section of a murine, before (baseline) and after 24-hour exposure to 50:50 nanoparticles

The optimized NP was injected intravenously (1 mL of 40 mg/mL) into a 200 g Wistar rat. The rat was euthanized 15 minutes after injection and the brain, liver, spleen and kidneys scanned by µCT. Only the calyces of the kidneys showed appreciable contrast which suggests renal clearance (Figure 15c).

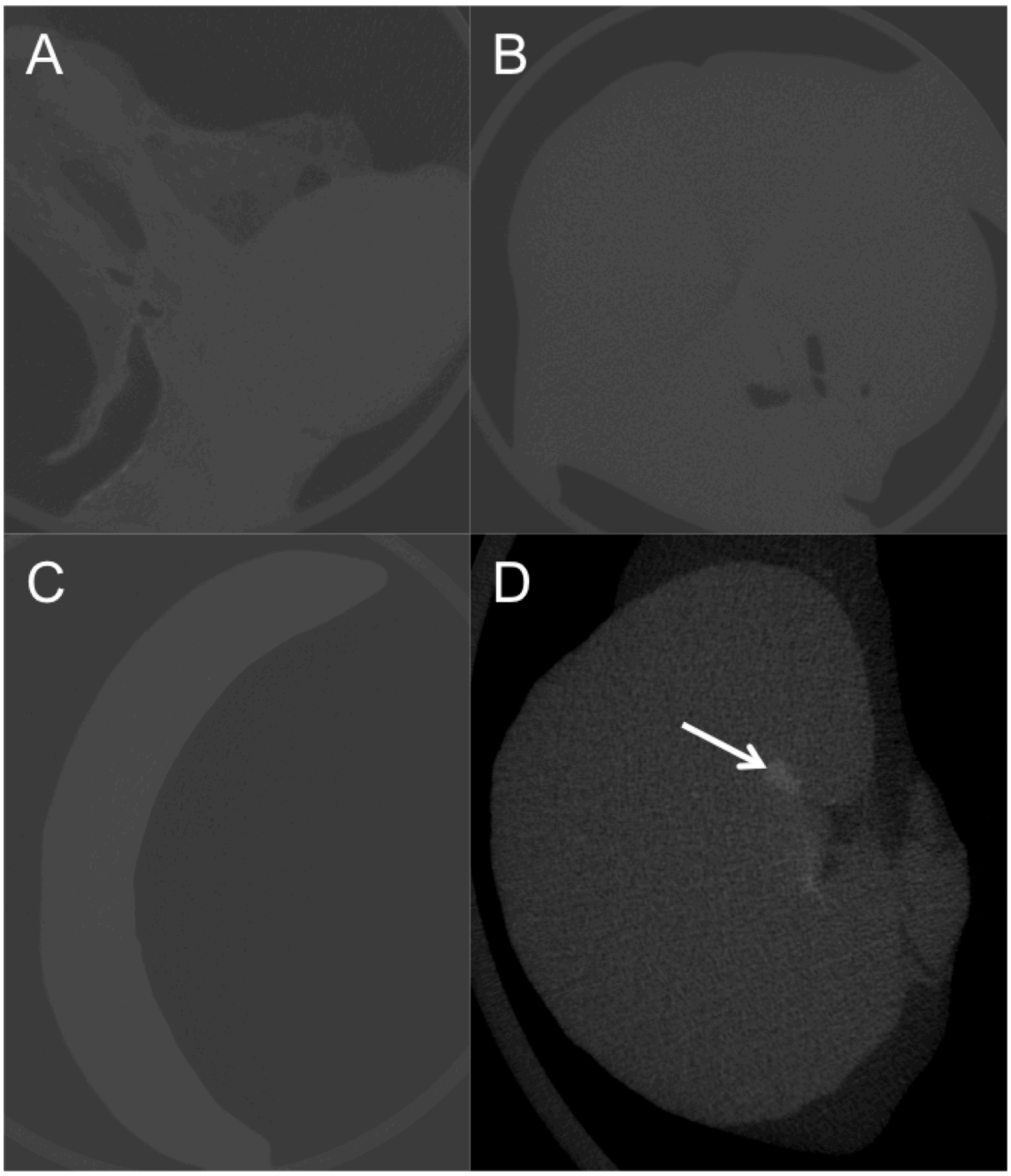

Figure S13c. CT images 15 minutes after injection of the 50:50 quaternary amine:pegylated Ta_2O_5 NPs. The brain (A), liver (B), and spleen (C) showed no appreciable contrast. The kidney (D) showed contrast in the calyces (arrow), suggesting renal clearance.

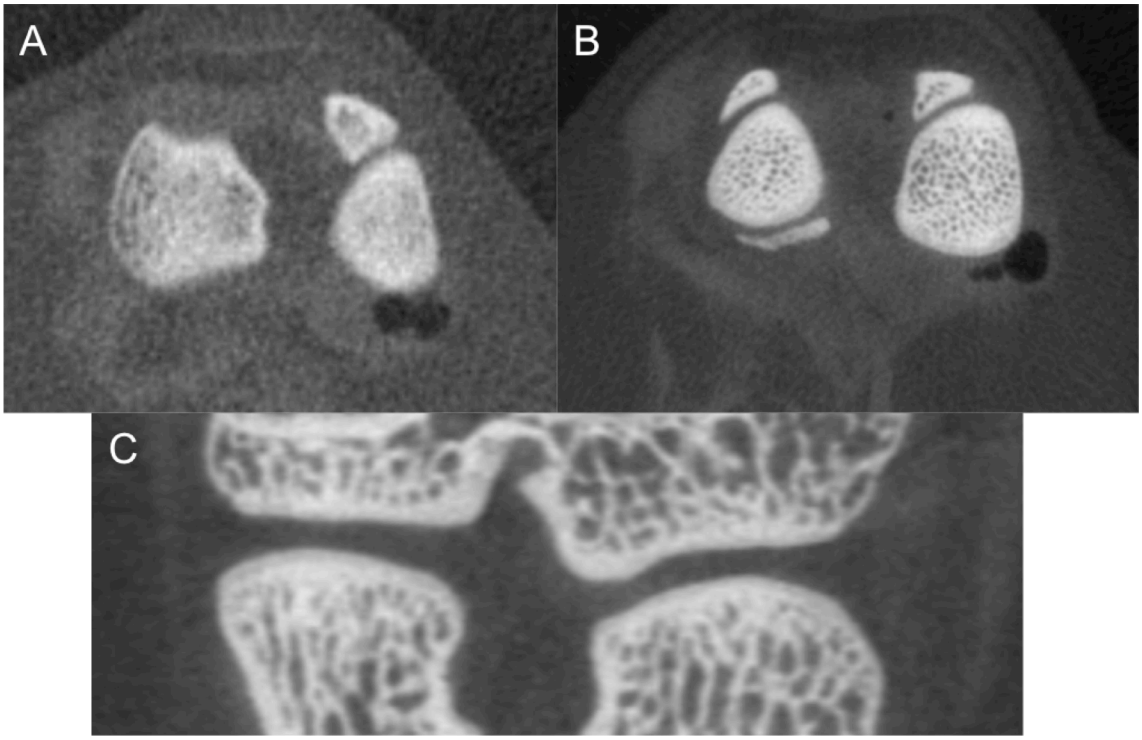

Figure S13d. Contrast enhanced CT images of a Wistar rat knee joint scanned *in vivo* (A) and *ex vivo* (B & C). The low resolution *in vivo* axial image (A) and high resolution *ex vivo* axial image (B) show contrast throughout the synovial space. Additionally, the coronal view is shown (C).

XIV. In Vivo & Ex Vivo Imaging of Rat Knee Joint using NP **2**

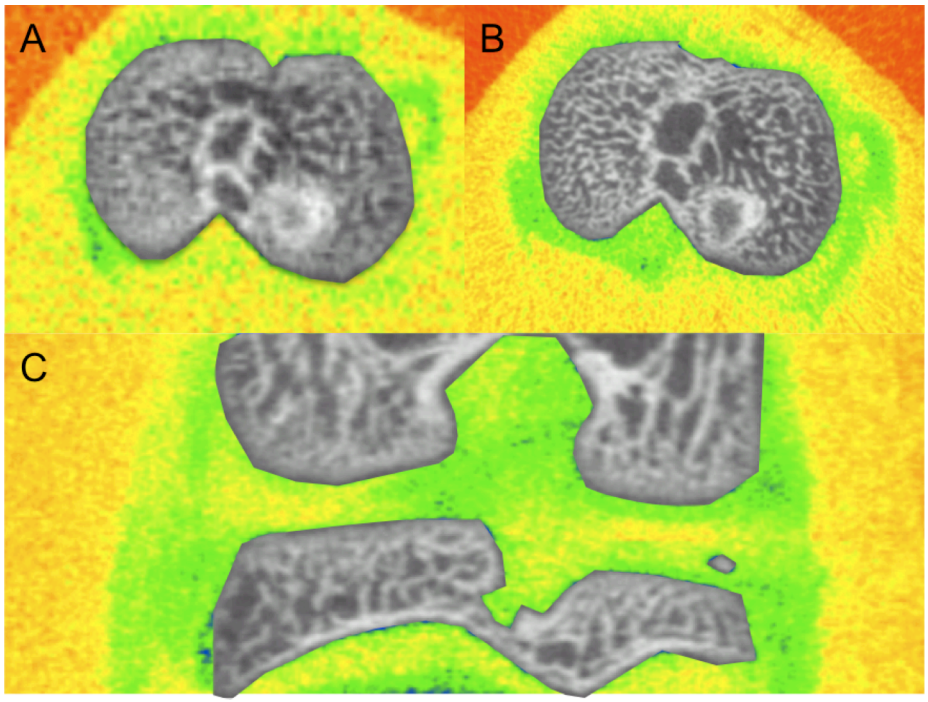

Figure S14a. A composite in vivo image (A) and ex vivo (B,C) showing the joint space in color and the bone in black in white. Contrast (green) can be seen throughout the joint compared to soft tissue, highlighting the cartilage (A, B) or cartilage, tendon, and meniscus (C).

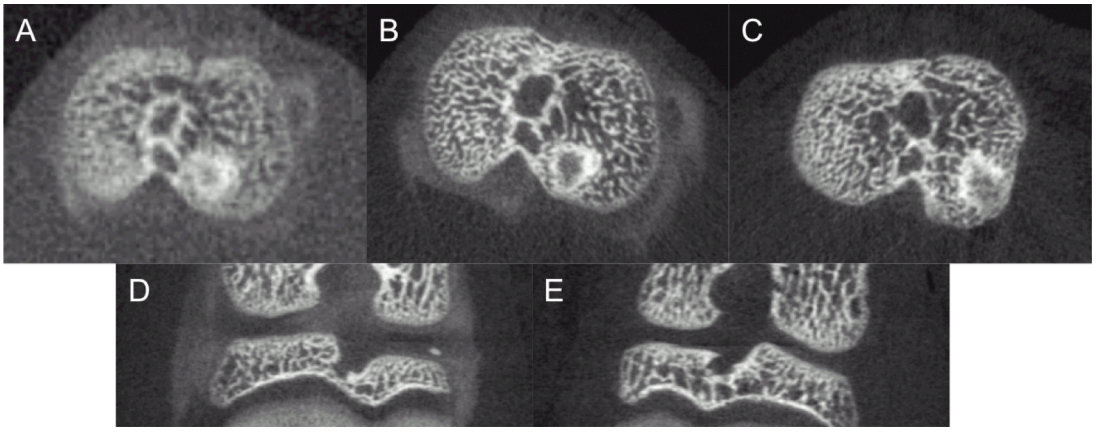

Figure S14b. Contrast enhanced CT images of a Wistar rat knee joint scanned *in vivo* (A) and *ex vivo* (B-E). The low resolution *in vivo* axial image (A) and high resolution *ex vivo* axial image (B) show contrast throughout the synovial space compared to the high resolution *ex vivo* axial image of the contralateral knee (C). Additionally, high resolution *ex vivo* coronal images show contrast throughout the joint (D) compared to the contralateral joint (E).

References

1 Oh, M. H. *et al.* Large-scale synthesis of bioinert tantalum oxide nanoparticles for X-ray computed tomography imaging and bimodal image-guided sentinel lymph node mapping. *J. Am. Chem. Soc.* **133**, 5508-5515, doi:10.1021/ja200120k (2011).

2 Bonitatibus, P. J., Jr., Torres, A. S., Goddard, G. D., FitzGerald, P. F. & Kulkarni, A. M. Synthesis, characterization, and computed tomography imaging of a tantalum oxide nanoparticle imaging agent. *Chem. Commun.* **46**, 8956-8958, doi:10.1039/c0cc03302b (2010).

3 Torres, A. S. *et al.* Biological performance of a size-fractionated core-shell tantalum oxide nanoparticle x-ray contrast agent. *Invest. Radiol.* **47**, 578-587, doi:10.1097/RLI.0b013e318260fc40 (2012).

4 Bonitatibus, P. J., Jr. *et al.* Preclinical assessment of a zwitterionic tantalum oxide nanoparticle X-ray contrast agent. *ACS Nano* **6**, 6650-6658, doi:10.1021/nn300928g (2012).